Iraqi Journal of Physics, 2025 *Vol.23, No.1, PP. 103-113*

https://doi.org/10.30723/ijp.v23i1.1359 *P-ISSN: 2070-4003*
E-ISSN: 2664-5548

An Investigation on the Rectifying Characteristics of PVA/Y_2O_3 Nanofibers

Ahmed J. Noori[1a*] and Iftikhar M. Ali[1b]
[1]*Department of Physics, College of Science, University of Baghdad, Baghdad, Iraq*
[a*]Corresponding author: ahmed.jumaah@sc.uobaghdad.edu.iq

Abstract

An electrospinning approach was used to synthesize composite nanofibers of polyvinyl alcohol (PVA) doped with different concentrations (2.5, 5, and 10 wt%) of Yttrium Oxide (Y_2O_3). The XRD diffraction pattern revealed a cubic structure of the prepared nanocomposite. The optical characteristics of pure PVA films and PVA/Y_2O_3 at different ratios were studied, where the energy gap decreases with the increase of Y_2O_3 concentration. The prepared samples' morphology and functional groups were characterized using field emission scanning electron microscopy (FESEM) and Fourier transform infrared (FTIR) spectrophotometry. FESEM images confirm the formation of well-defined nanofibers with variations in fibre diameter as the Y_2O_3 content increases, while FTIR spectra reveal characteristic functional groups associated with both PVA and Y_2O_3. Finally, the current-voltage (I-V) characterization of PVA and PVA/ Y_2O_3 was measured at room temperature showing the non-Ohmic behaviors. The result indicates potential applications in electronic and sensing devices.

Article Info.

Keywords:
Electrospinning, Polyvinyl Alcohol, Yttrium Oxide, Nanofibers, Rectifier.

Article history:
Received: Aug. 30, 2024
Revised: Nov. 12, 2024
Accepted: Des. 12, 2024
Published: Mar 01,2025

1. Introduction

The synthesis of polymers has drawn a lot of attention in recent years [1]. The development of photovoltaic devices through new technologies, materials, and processes has attracted much attention lately as the potential for cost savings and increased efficiency. One such processing technique is synthesizing different semiconductor nanocrystalline layers for device application using polymer matrices as a capping agent. Polymer-capped semiconductor layers could adjust their physical characteristics, especially optical and electrical ones [2]. Water-soluble synthetic polymer PVA is widely known for its advantageous attributes, which include low cost, non-toxicity, ease of manufacture, high optical transparency, strong chemical stability, good biocompatibility, and outstanding mechanical qualities [3]. Nanotechnology is a fast-advancing and expanding field that has garnered increasing media attention and public interest over the past decade. It has wide-ranging applications in various research areas, development, and industrial. The focal point of all these programs is the advancement of novel nanomaterials. It is well-established that adding inorganic substances to polyvinyl alcohol (PVA) alters its characteristics. It is very important to the field of science [4]. Polymer composite materials are widely used in several industries due to their superior mechanical properties to granular or ceramic composites. These properties include enhanced tensile strength, elastic modulus, and flexibility. Composites possess remarkable qualities such as high hardness, high melting point, low density, low coefficient of thermal expansion, high thermal conductivity, excellent chemical stability, and improved mechanical properties, including high specific strength, enhanced wear resistance, and specific modulus. These exceptional characteristics make composites highly suitable for various industrial applications. Composites are employed in producing solar cells, laser diodes, light-emitting diodes (LEDs), and optoelectronic device components [5].

Metal-oxide nanomaterials are emerging prospects in various fields, such as chemistry, materials science, physics, and biotechnology, and the specific electrical configuration dictates the conductive, semiconductive, and insulative characteristics of nanomaterials. Transition metal ions generally have partially filled d-shells, which enables them to undergo reactive electronic transitions. This property also contributes to their broad band gaps, outstanding electrical properties, and high dielectric constant [6].

The properties of surface-dependent nanomaterials, such as optics, mechanics, electricity, magnetism, and catalysis, are primarily influenced by the nanostructured metal oxides' dimensions and shape. The deliberate modification of nanostructures for MOx design and enabling adjustable features has garnered significant interest in pursuing an expanded range of effectiveness in biomedicine, industries, and other domains. It has stimulated research endeavors to modify nanomaterials with morphologically controlled structures and uniformly sized pores to achieve specific functionalities [7]. Yttrium oxide (Y_2O_3) is highly significant in several technical applications due to its ability to remain stable under light exposure, its capacity for redox reactions, and its electromagnetic properties. Y_2O_3 nanoparticles, with their small size, strong luminescence, and exceptional physical-chemical stability, have found applications in removing organic contaminants, biological activities, supercapacitors, and biomedical and live-cell imaging. In addition, Y_2O_3 nanoparticles can undergo a reaction with the organic framework, resulting in the formation of surface organometallic fragments. This process enhances the photoelectrical activity in light emitters [8].

This study presents a novel application of electrospinning technique to produce composite nanofibers of PVA mixed with different amounts of Y_2O_3. The study primarily examines the optical characteristics of these films, specifically the effect of elevated Y_2O_3 concentration on the energy gap. Advanced characterisation techniques, such as field emission scanning electron microscopy (FESEM) and Fourier transform infrared spectroscopy (FTIR), were utilized to examine the morphology and content of the nanofibers. Although extensive research has concentrated on improving the mechanical and chemical properties of analogous materials, limited studies examine their electrical properties, including rectification behaviour, in optoelectronic applications. This study focuses to address this gap by investigating the impact of Y_2O_3 nanoparticle integration on the optoelectronic properties of PVA nanofibers, highlighting their potential for advanced device applications.

2. Experimental Work

2. 1. Materials

4 gm of PVA was added to a beaker filled with 4 ml of distilled water under magnetic stirring for 7 h and heated to about 70 °C. Next, different weight percentages of Y_2O_3 (2.5, 5, and 10 Wt.%) of average particle size of 100nm were added to the PVA solution to produce PVA/Y_2O_3 composite.

2. 2. Thin Film Preparation

The electrospinning process was employed to obtain clean and doped samples under the following ideal conditions: a direct current (D.C) voltage of 15kV, a flow rate of 0.1 ml/h, and a distance of 16cm between the collector and tip needle.

3. Results and Discussion

3. 1. X-Ray Diffraction

The XRD patterns of Y_2O_3 nanoparticles, as depicted in Fig. 1, closely match those on the JCPD card 00-041-1105 and are consistent with the data provided in the literature [3, 9]. This indicates that the synthesized Y_2O_3 nanoparticles have a cubic

lattice structure. The crystallite size was determined using the Scherrer formula, where D= 78.7nm for pure Y_2O_3.

Fig. 2 displays the X-ray diffraction (XRD) patterns of the pure PVA and PVA-Y_2O_3 composite of different weight percentages of Y_2O_3. The XRD pattern closely matches that on the ICSD card no 00-041-1105, confirming the cubic lattice structure of the composite. These findings agree with previous research [9, 10]. The X-ray diffraction (XRD) pattern of 4wt.%PVA/2.5wt.%Y_2O_3 displays peaks corresponding to (200), (332), (440), (311), (800). The 4wt.%PVA/5wt.%Y_2O_3 XRD pattern peaks corresponds to (211), (440), (600), (611), (642), (811). While those of 4wt.%PVA/10wt.% Y_2O_3 corresponds to (211), (440), (600), (611), (642), (811). The exact locations of the peaks and their accompanying Miller indices for the diffracting planes, along with the Full Width at Half Maximum (FWHM) measurements, were determined and analyzed to characterize the crystal structure. The average crystalline' s size decreased from 36.11 nm to 15.2 nm when Y_2O_3 concentration increased from 2.5wt% to 10wt%.

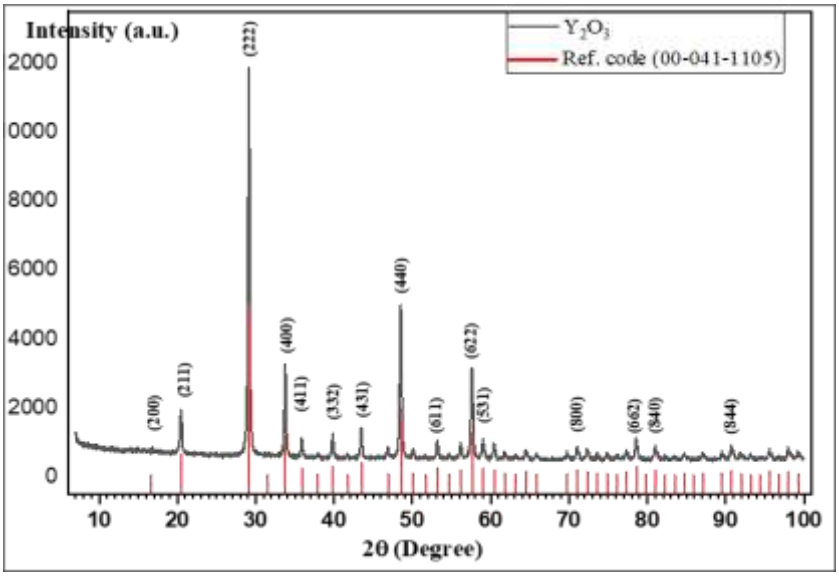

Figure 1: X-ray diffraction pattern of Y_2O_3.

The undoped and doped PVA patterns exhibit no differences, suggesting a uniform nano PVA/Y_2O_3 distribution. The absence of prominent peaks indicates that the PVA nanofibers are primarily amorphous [9, 11].

The pure PVA diffraction pattern exhibited a diffraction band at an angle of 24˚; the peaks observed are attributed to the crystalline structure of the PVA polymer molecules. These peaks may result from strong hydrogen bonding between the PVA chains within and between the molecules [3, 12]. Figs. 1 and 2 show the exact locations of the peaks and their accompanying Miller indices for the diffracting planes.

The crystallite size can be determined using the Scherrer formula [13]:

$$D = \frac{K\lambda}{\beta \cos\theta} \qquad (1)$$

where λ represents the wavelength of X-rays, θ represents the diffraction angle, and β represents the adjusted full width at half maximum. The average crystalline size value of the nanoparticles was determined in the range (36.11-15.2) nm [2].

Average crystallite size decreased with the increase of the weight percentage of Y_2O_3. The Y_2O_3 concentration increase may result in crystallite dispersion or disturb the crystalline arrangement. Dopants can introduce defects in the polymer crystalline lattice

or impede full crystallite development, leading to reduced crystallite sizes and heightened lattice inhomogeneity.

The decrease of crystallite size with different Y_2O_3 doping increases surface area, hence improving humidity sensitivity, optical tunability, and perhaps flexibility. These modifications enhance the material's appropriateness for sensors, optoelectronics, and applications requiring significant surface interactions.

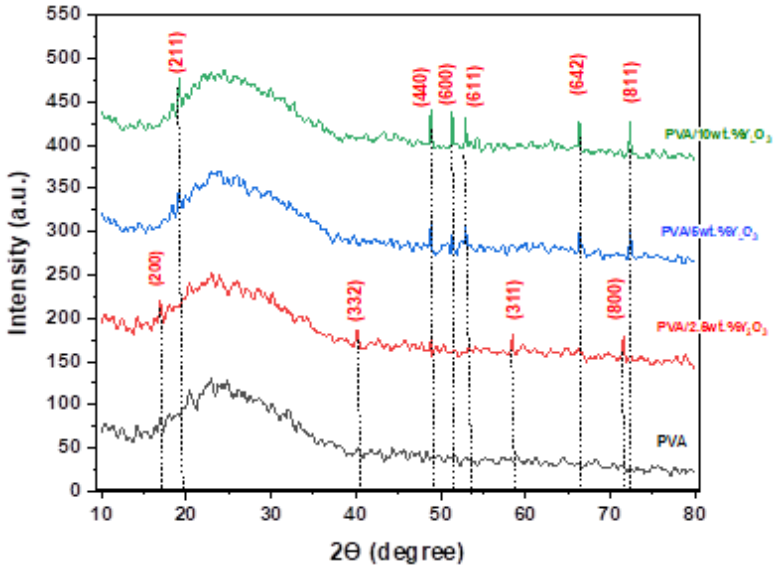

Figure 2: XRD patterns of PVA and PVA/Y_2O_3 nanocomposites with varying Y_2O_3 concentrations.

3. 2. The Optical Characteristics

Fig. 3 displays the absorption spectra of pure PVA and Y_2O_3 composite nanofiber samples fabricated using electrospinning. When the amount of additional Y_2O_3 nanoparticles in (PVA/Y_2O_3) nanocomposites increased, an increase in the absorption coefficient was noted. This increase is attributed to the increased Y_2O_3 nanoparticle carrying charges, which raises absorbance.

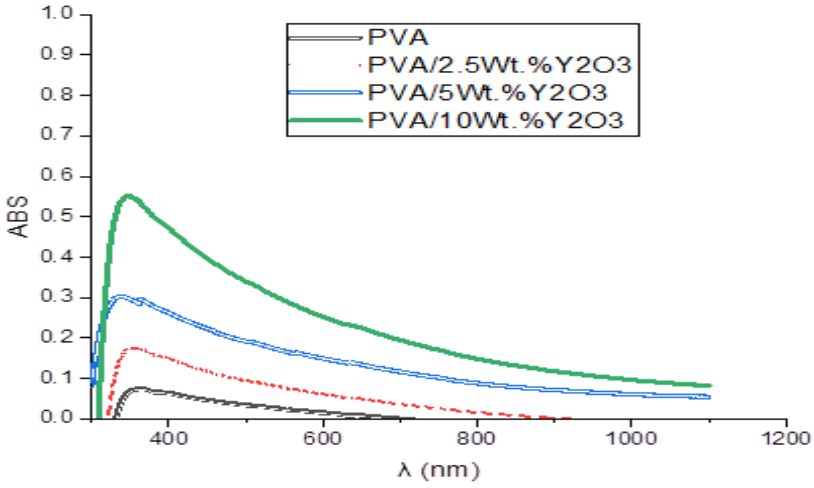

Figure 3: The absorption spectra of pure PVA and PVA/Y_2O_3 composite.

The optical absorption coefficient (α), according to the Beer-Lambert law, can be determined:

$$\alpha = \frac{2.303 \times A}{t} \qquad (2)$$

where (t) is the sample thickness and (A) is the optical absorbance (A) [14, 15]. Tauc's formula was used to determine the optical bandgap:

$$\alpha h\upsilon = C(h\upsilon - E_g)^r \quad (3)$$

where hν is the energy of the input photon, E_g is the optical energy band, and C is a constant that varies with the material structure. The exponent (r) defines the electronic transition; it equals 0.5 for direct transition [16, 17].

Fig. 4 illustrates Tauc plots for the pure PVA and the three created PVA/Y_2O_3 nanocomposite films, from which the band gap can be obtained. Y_2O_3 dispersion in the PVA matrix reduces the optical band gap, going from 2.65 eV for pure PVA to 2.3 eV for 10 Wt.% Y_2O_3-PVA. When the concentration of the Y_2O_3 nanoparticle was increased the optical band gap of the films decreased [18]. This result agrees with that of Alrowaili et al. [9] and El-Sayed et al. [19].

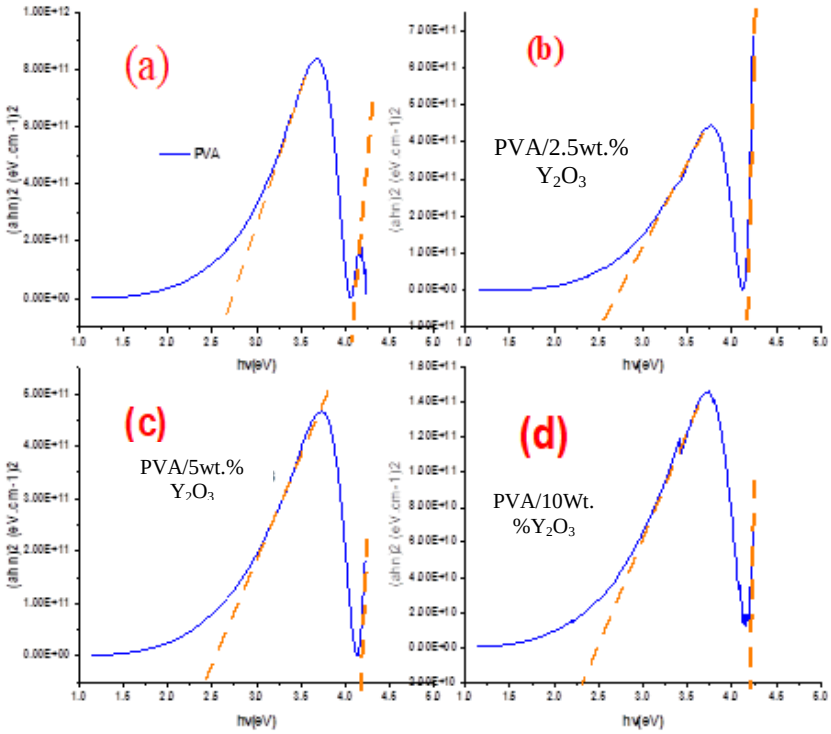

Figure 4: The relationship between $(\alpha h\upsilon)^2$ and the energy (hυ) for (a) pure PVA, (b) 2.5wt%, (c) 5wt%, and (d) 10 wt% of PVA/Y_2O_3 nanocomposites.

The band gap energy of the B band remains consistently stable regardless of the varying percentages of Y_2O_3 doping, showing only minimal increases or no changes. The stability of the B band suggests that it exhibits a lower level of responsiveness to doping compared to the Q band.

Any change in the band gap values of the nano-Y_2O_3 loaded PVA composite films could result from a complex formed when the polar (hydroxyl) groups of PVA interact with Y_2O_3 NPs. PVA chains become rigid due to this complicated development, which may result in cross-linking [20].

Decrease in optical band gap induces a doping effect in the overall structure of the PVA material, generating new energy levels inside the initial band gap. This results in a diminished optical band gap since photons may now promote electrons to these lower-energy states, reducing the energy necessary for electronic transitions.

3. 3. Field Emission Scanning Electron Microscopy

The morphology of electrospinning nanofibers is shown in Fig. 5. An FESEM images of pure PVA, PVA/2.5wt.%Y_2O_3, and PVA/10wt.%Y_2O_3 shows nanofibers of a regular average diameter of about 131 nm, indicating a homogenous and smooth shape**.**

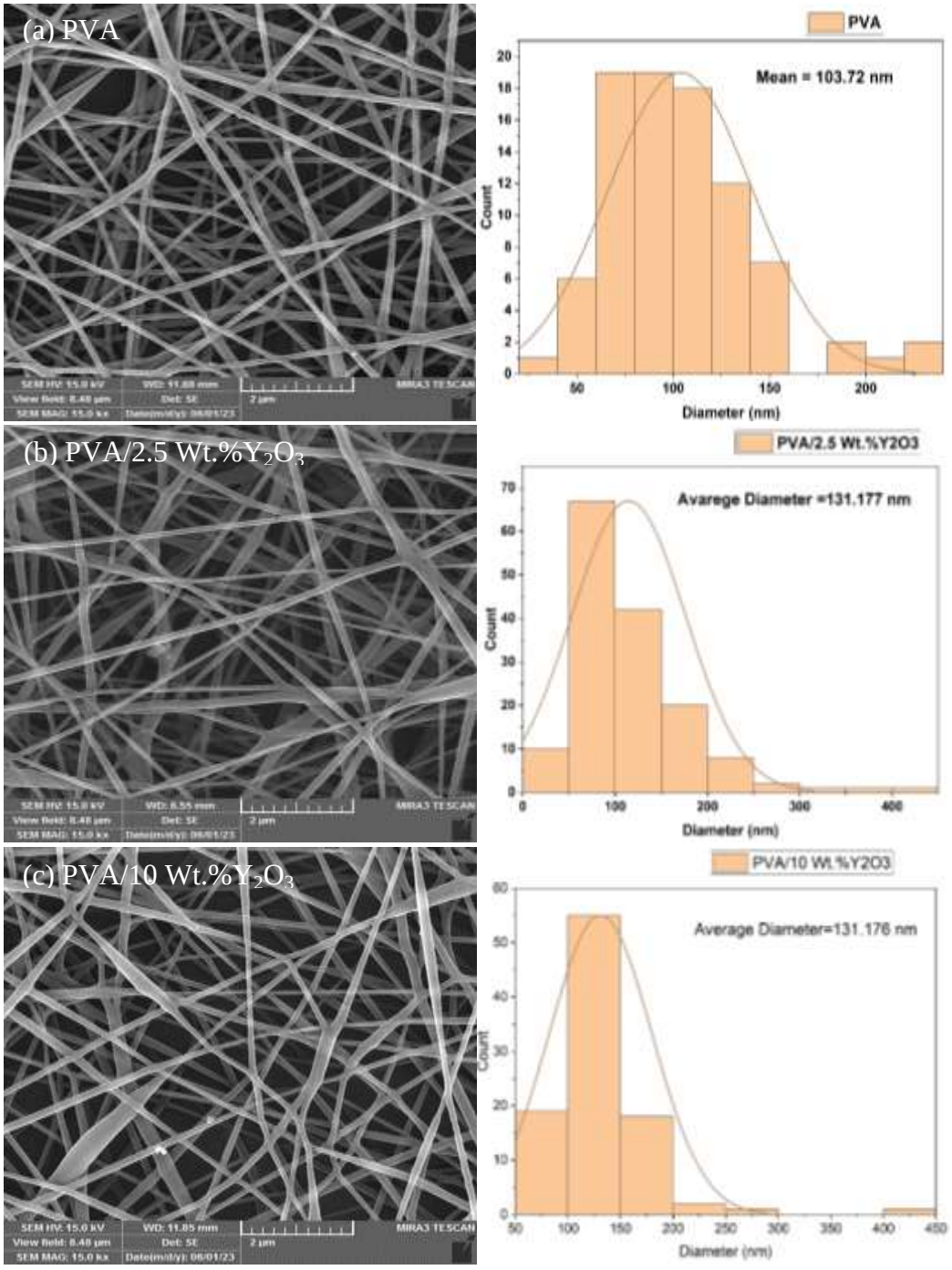

Figure 5: FESEM image of (a) pure PVA, (b) 2.5wt%, and (c) 10 wt% of PVA/Y_2O_3 nanocomposites.

3.4. Fourier-Transform Infrared Spectroscopy

FTIR spectroscopy is a necessary method for examining the band structure of materials, which varies according to their composition. It has the potential to unveil the intricacy and interplay of different constituents, such as polymers, ions, and cations [21]. Fig. 6 displays the FTIR spectra for pure PVA and PVA/Y_2O_3 nanofiber. The data reveals distinct absorption bands that indicate the presence of hydrophobic (CH-) and

hydrophilic (CO-) functional groups [22]. The samples exhibited a wide spectral range between 3554 cm^{-1} and 3600 cm^{-1}, attributed to the stretching vibration of O-H in the hydroxyl groups. The C-H bands were observed in the 3050–3255/cm^{-1} range [23]. Whereas the C-O wide bands were observed in the range of 1000-1500/cm^{-1}. A triple bond region 2000-2500 cm^{-1} was identified, suggesting the presence of a C ≡ C bond in the material [24]. The spectra obtained exhibit an absorbed band at around 580-650cm^{-1}, which indicates the distinctive band associated with the monoclinic phase of pure Y_2O_3(metal oxygen) [25].

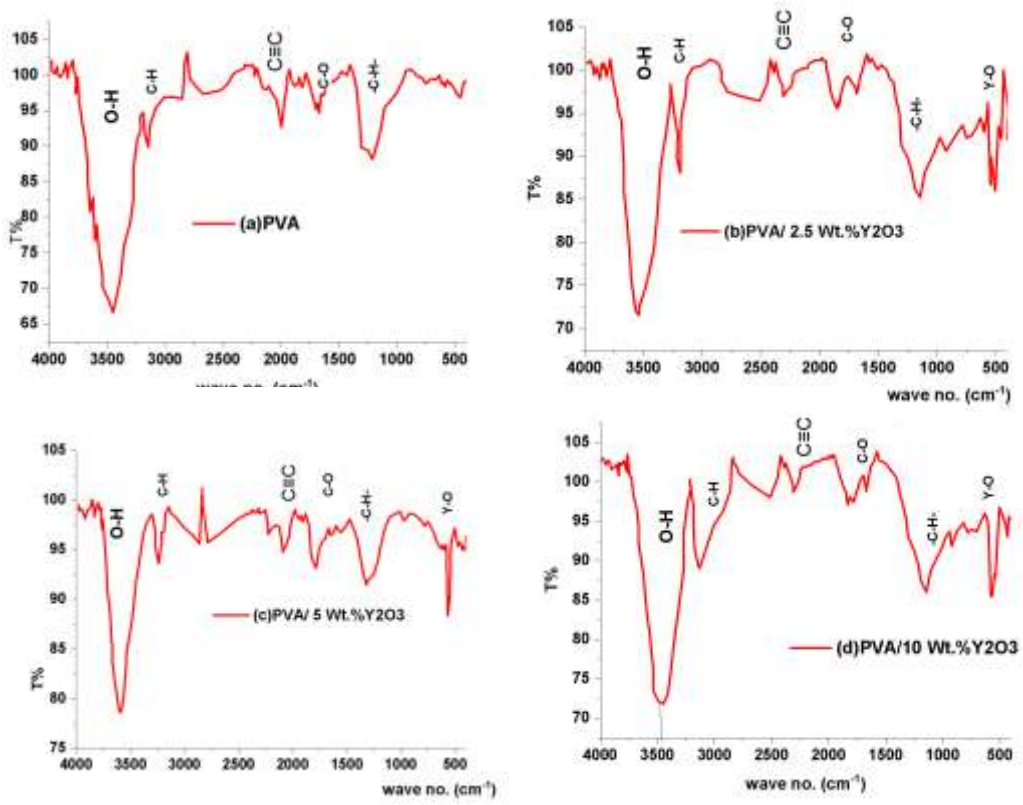

Figure 6: FTIR spectra for (a) pure PVA, (b) 2.5wt%, (c) 5wt%, and (d) 10 wt% of PVA/Y_2O_3 nanocomposites.

3. 5. Current-Voltage (I-V) Characteristics

Photoconductivity is a significant technique for examining how materials conduct electricity in response to light and obtaining valuable insights into photo-excitation characteristics. It also heavily relies on carrier density and carrier production, trapping, and recombination processes [26]. The built-in potential between PVA-Y_2O_3 and aluminum allowed the PVA-Y_2O_3 nanocomposite to observe the electrical transport property. The following equation was used to determine the barrier high Φ_b [8]:

$$\Phi_b = \frac{KT}{q}\left(\frac{AA^*T^2}{I_s}\right) \quad \textbf{(4)}$$

where K is Boltzmann constant, T is the absolute temperature, A is the effective area, A* Richardson's constant, q is the electron charge, and I_s is the saturation current.

Fig. 7 shows the current-voltage (I–V) characteristic curves for the sandwich structure of PVA-Y_2O_3/Al under dark and light (with white light of an intensity of 105 mW/cm^2,132 mW/cm^2, and 183 mW/cm^2) conditions. It illustrates the rectifying behavior of the characteristic curves, which suggests the Schottky nature. The I-V of pure PVA curves showed a degree of symmetry between the applied voltage's positive

and negative. The lowest current occurs in the dark, whereas the maximum current was measured at 183 mW/Cm^2.

Fig. 8 and Table 1 provide the Ln J vs. V curves for the samples under study. Fig. 8 demonstrates that each feature has two different zones. The linear behavior is caused by a conduction process similar to an electronic one. Heat activation across the potential barrier releases the charge carriers in this case [27]. From Table 1, it can be noted that the potential barrier (Φ_b) decreased with the increase in the Y_2O_3 concentration. There are two explanations for the physical characteristics of such a potential barrier. It might be the charge carriers' passage between the dielectric and cathode barriers (Schottky emission). Alternatively, the charge carriers can be freed into the dielectric from traps (The Poole-Frenkel effect) [28]. Usually, better nonlinear characteristics correspond with higher values of Φ_b. Concurrently, the probabilities of the interface state density vary [29]. Regarding the pure PVA sample, the photocurrent measurements, which generally increase as the irradiance level increases, demonstrating a positive correlation between irradiance and photocurrent. As the concentration of Y_2O_3 doping was increased, photocurrent increased significantly at all irradiation intensities. This suggests that Y_2O_3 doping enhances the photocurrent responsiveness of PVA nanofibers. However, at the highest irradiation level (183 mW/cm^2), the photocurrent of the PVA/ 10wt.% Y_2O_3 sample was notably more considerable than that of the other samples. It may indicate that this is the optimal doping concentration to optimize photocurrent in high-irradiance environments.

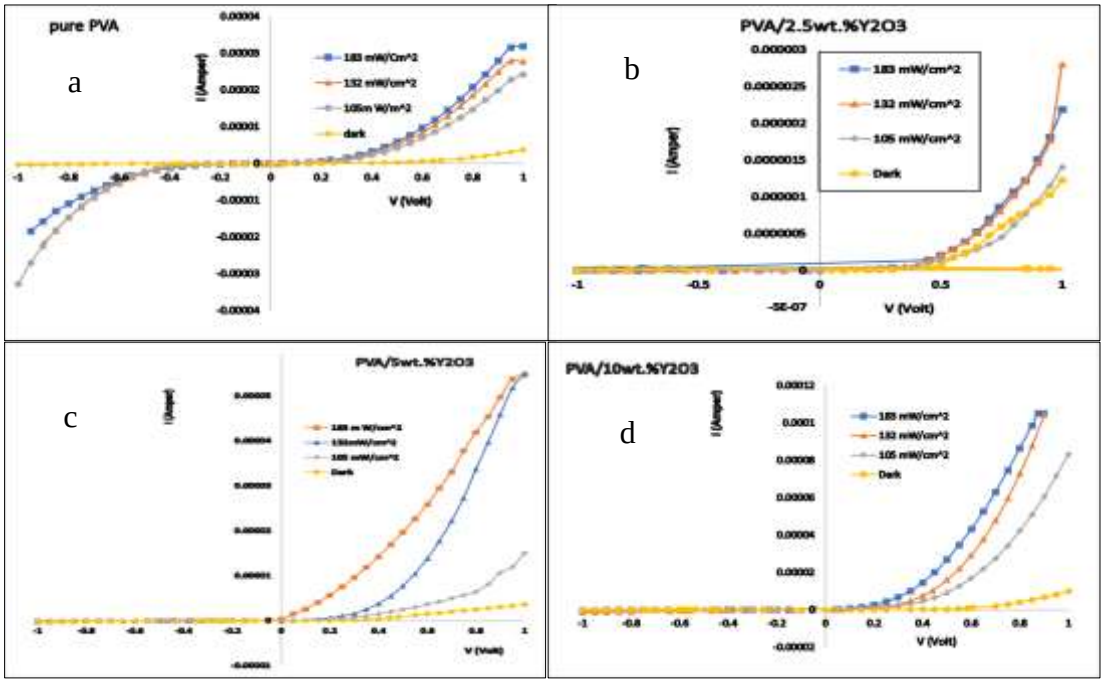

Figure 7: Current I (A) vs. voltage V (V) characteristics under dark and light at the different densities of energy for (a)pure PVA, (b) 2.5wt%, (c) 5wt%, and (d) 10 wt% of PVA/Y_2O_3 nanocomposites..

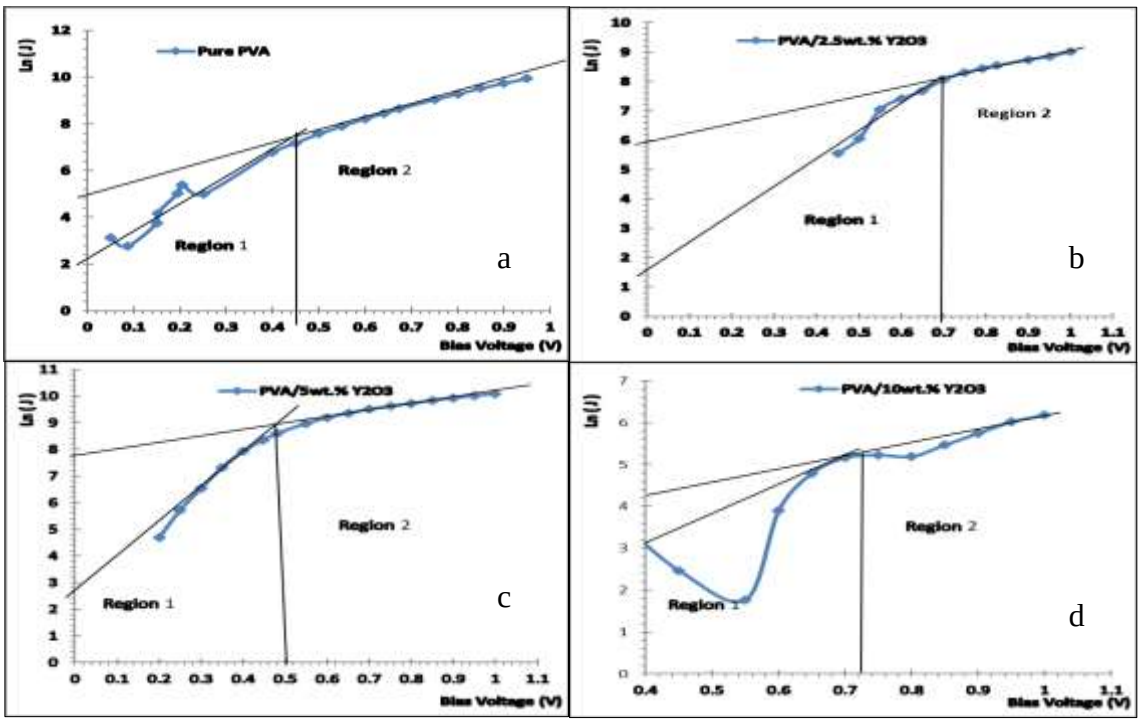

Figure 8: Ln(J) vs. bias voltage (V) for (a) pure PVA, (b) 2.5wt%, (c) 5wt%, and (d) 10 wt% for PVA/Y_2O_3 nanocomposites.

Table 1: The values of built-in voltage (Φ_b) 2.5, 5, and 10 wt% of PVA/ Y_2O_3 nanocomposite.

Sample	built-in voltage (Φ_b) (V)
PUR PVA	0.91
PVA/2.5 Wt.% Y_2O_3	0.88
PVA/ 5 Wt.% Y_2O_3	0.87
PVA/ 10Wt.% Y_2O_3	0.86

4. Conclusions

XRD diffraction, scanning electron microscopy, Fourier transform infrared spectroscopy, optical absorption spectroscopy, and current-voltage (I_V) studies have all been used to investigate the impact of Y_2O_3 nanoparticles on ordinary PVA films. The Y_2O_3 nanoparticles have a cubic crystal structure with the average size of the crystals between 36 and 17.7 nm. The dispersion of Y_2O_3 nanoparticles indicates the uniform and smooth morphology of the PVA polymer surface. The FTIR spectra showed potential interactions between the host PVA sheets and Y_2O_3 nanoparticles. As the concentration of Y_2O_3 in the PVA/Y_2O_3 nanocomposite thin film increased, the optical energy gaps decreased at different concentrations. Adding Y_2O_0 nanoparticles makes the average diameter of PVA bigger, probably because the structure of the matrix changes. There was some symmetry between the positive and negative voltages in the I-V curves of pure PVA-only curves. In the future, researchers may focus on using Y_2O_0-doped PVA films in humidity sensors or optoelectronic devices to make them more useful in real life. Subsequent research may also investigate their stability and scalability.

Acknowledgments

Thin film laboratories and the physics departments of the College of Science at Baghdad University provided support for this endeavour. We acknowledge the support provided by the entire staff at these laboratories.

Conflict of Interest

The authors declare that they have no conflict of interest.

References

1. R. H. Almuswy and A. H. Ahmad, Iraqi J. Phys. **20**, 13 (2022). DOI: 10.30723/ijp.v20i3.1008.
2. H. M. Alhusaiki Alghamdi, Opt. Mat. **134**, 113101 (2022). DOI: 10.1016/j.optmat.2022.113101.
3. Y. R. Kumar, J. G. Thangamani, T. K. Karthik, K. Deshmukh, and S. K. Pasha, RSC Adv. **14**, 5022 (2024). DOI: 10.1039/D3RA04257J.
4. A. Manjunath, M. Irfan, K. P. Anushree, K. M. Vinutha, and N. Yamunarani, Adv. Mat. Phys. Chem. Mat. **6**, 263 (2016). DOI: 10.4236/ampc.2016.610026.
5. M. H. Abbas, A. Hadi, B. H. Rabee, M. A. Habeeb, M. K. Mohammed, and A. Hashim, J. Comp. Adv. Mat. **33**, 261 (2023). DOI: 18280/rcma.330407.
6. Y. Yoon, P. L. Truong, D. Lee, and S. H. Ko, ACS Nanosci. Au **2**, 64 (2022). DOI: 10.1021/acsnanoscienceau.1c00029.
7. Z. Alhalili, Molecules **28**, 3086 (2023). DOI: 10.3390/molecules28073086.
8. M. A. Siddiq, M. Sopaih, and E. Elgazzar, ACS Omega **8**, 24883 (2023). DOI: 10.1021/acsomega.3c00962.
9. Z. A. Alrowaili, T. A. Taha, K. S. El-Nasser, and H. Donya, J. Inorg. Organomet. Poly. Mat. **31**, 3101 (2021). DOI: 10.1007/s10904-021-01995-2.
10. Q. Cheng, V. Pavlinek, C. Li, A. Lengalova, Y. He, and P. Saha, Appl. Surf. Sci. **253**, 1736 (2006). DOI: 10.1016/j.apsusc.2006.03.004.
11. M. Rashad, Opt. Mat. **105**, 109857 (2020). DOI: 10.1016/j.optmat.2020.109857.
12. R. Ricciardi, F. Auriemma, C. De Rosa, and F. Lauprêtre, Macromolecules **37**, 1921 (2004). DOI: 10.1021/ma035663q.
13. M. I. Hasan, N. A. Bakr, and I. M. Ibrahim, J. Electron. Mater. **50**, 2716 (2021). DOI: 10.1007/s11664-021-08790-2.
14. F. K. Jawad and N. a. A. Al-Tememee, Iraqi J. Sci. **64**, 4436 (2023). DOI: 10.24996/ijs.2023.64.9.13.
15. Q. M. Al-Bataineh, A. M. Alsaad, A. A. Ahmad, and A. Telfah, Heliyon **6**, e04177 (2020). DOI: 10.1016/j.heliyon.2020.e04177.
16. A. M. Al-Fa'ouri, O. A. Lafi, H. H. Abu-Safe, and M. Abu-Kharma, Arabian J. Chem. **16**, 104535 (2023). DOI: 10.1016/j.arabjc.2022.104535.
17. N. K. Abbas, Z. J. Shanan, and T. H. Mohammed, Baghdad Sci. J. **19**, 0217 (2022). DOI: 10.21123/bsj.2022.19.1.0217.
18. K. Sk, V. N, B. Rb, and S. Madivalappa, Sol. St. Commun. **370**, 115221 (2023). DOI: 10.1016/j.ssc.2023.115221.
19. F. El-Sayed, M. I. Mohammed, and I. S. Yahia, J. Mater. Sci. Mater. Electron. **31**, 10408 (2020). DOI: 10.1007/s10854-020-03589-z.
20. M. Aslam, M. A. Kalyar, and Z. A. Raza, Polym. Bull. **78**, 1551 (2021). DOI: 10.1007/s00289-020-03173-9.
21. F. Aljubouri and M. Kadhim Jawad, Iraqi J. Phys. **21**, 1 (2023). DOI: 10.30723/ijp.v21i1.1093.
22. J. H. Taha, N. K. Abbas, and A. A. Al-Attraqchi, Int. J. Drug Deliv. Tech. **10**, 378. DOI: 10.25258/ijddt.10.3.13.
23. Z. K. Heiba, M. B. Mohamed, S. I. Ahmed, and A. A. Alhazime, J. Vinyl. Addit. Technol. **27**, 410 (2021). DOI: 10.1002/vnl.21815.
24. A. B. D. Nandiyanto, R. Oktiani, and R. Ragadhita, Indonesian J. Sci. Tech. **4**, 97 (2024). DOI: 10.17509/ijost.v4i1.15806.
25. N. R. Dhineshbabu, V. Rajendran, N. Nithyavathy, and R. Vetumperumal, Appl. Nanosci. **6**, 933 (2016). DOI: 10.1007/s13204-015-0499-2.
26. F. M. Ali, I. M. Ashraf, and S. M. Alqahtani, Phys. B Cond. Matt. **527**, 24 (2017). DOI: 10.1016/j.physb.2017.09.107.
27. A. M. El Sayed, S. El-Gamal, W. M. Morsi, and G. Mohammed, J. Mater. Sci. **50**, 4717 (2015). DOI: 10.1007/s10853-015-9023-z.
28. I. Jabbari, M. Baira, H. Maaref, and R. Mghaieth, Sol. St. Commun. **314-315**, 113920 (2020). DOI: 10.1016/j.ssc.2020.113920.
29. C.-W. Nahm, J. Korean Ceram. Soc. **55**, 504 (2018). DOI: 10.4191/kcers.2018.55.5.10.

دراسة حول خصائص التقويم لألياف النانو PVA/Y_2O_3

احمد جمعة نوري[1] وافتخار على محمود[1]
[1] قسم الفيزياء، كلية العلوم، جامعة بغداد، بغداد، العراق

الخلاصة

تم استخدام تقنية الغزل الكهربائي لتصنيع ألياف نانوية مركبة من بولي فينيل الكحول (PVA) المشوب بأكسيد الإيتريوم (Y_2O_3) بتركيزات مختلفة (2.5، 5، و10 وزن٪). وكشف نمط حيود الأشعة السينية (XRD) عن بنية مكعبة للمركب النانوي المحضر. تم دراسة الخصائص البصرية لأغشية PVA النقية وPVA/Y_2O_3 بنسب مختلفة، حيث وُجد أن فجوة الطاقة تنخفض مع زيادة تركيز Y_2O_3. كما تم تحليل البنية المورفولوجية والمجموعات الوظيفية للعينات المحضرة باستخدام مجهر المسح الإلكتروني بالإصدار الميداني (FESEM) ومطياف الأشعة تحت الحمراء بتحويل فورييه (FTIR)، على التوالي. أكدت صور FESEM تكوين ألياف نانوية محددة جيدًا مع تباين في قطر الألياف عند زيادة محتوى Y_2O_3، بينما كشفت أطياف FTIR عن المجموعات الوظيفية المميزة لكل من PVA وY_2O_3. وأخيرًا، تم قياس خصائص التيار-الجهد (I-V) لأغشية PVA وPVA/Y_2O_3 عند درجة حرارة الغرفة باستخدام مقياس كهربائي، حيث أظهرت النتائج سلوكًا غير أومي، مما يشير إلى إمكانية استخدامها في التطبيقات الإلكترونية وأجهزة الاستشعار.

الكلمات المفتاحية: الغزل الكهربائي، بولي فاينيل الكحول، أكسيد الإيتريوم، الألياف النانوية، المواد المركبة، المقوم.